frontiers | Frontiers in Natural Products

TYPE Original Research
PUBLISHED 26 June 2023
DOI 10.3389/fntpr.2023.1190053

OPEN ACCESS

EDITED BY
Michał Tomczyk,
Medical University of Bialystok, Poland

REVIEWED BY
Daniel Rinaldo,
São Paulo State University, Brazil
Alan Talevi,
National University of La Plata, Argentina

*CORRESPONDENCE
Eduardo Munoz,
fi1muble@uco.es
Diego Caprioglio,
diego.caprioglio@uniupo.it

RECEIVED 20 March 2023
ACCEPTED 12 June 2023
PUBLISHED 26 June 2023

CITATION
Amin HIM, Ruiz-Pino F, Collado JA, Appendino G, Tena-Sempere M, Munoz E and Caprioglio D (2023), Synthesis and biological evaluation of hydroxamate isosteres of acidic cannabinoids. *Front. Nat. Produc.* 2:1190053. doi: 10.3389/fntpr.2023.1190053

Synthesis and biological evaluation of hydroxamate isosteres of acidic cannabinoids

Hawraz Ibrahim M. Amin[1], Francisco Ruiz-Pino[2], Juan A. Collado[2], Giovanni Appendino[1], Manuel Tena-Sempere[3,4,5,6], Eduardo Munoz[3,4,5]* and Diego Caprioglio[1]*

[1]Università del Piemonte Orientale, Dipartimento di Scienze del Farmaco, Novara, Italy, [2]VivaCell Biotechnology España, Córdoba, Spain, [3]Maimonides Biomedical Research Institute of Cordoba, Córdoba, Spain, [4]Department of Cellular Biology, Physiology and Immunology, University of Cordoba, Córdoba, Spain, [5]Reina Sofía University Hospital, Córdoba, Spain, [6]CIBER Fisiopatología de la Obesidad y la Nutrición (CIBEROBN), Instituto de Salud Carlos III, Córdoba, Spain

Despite their early discovery, the bioactivity of acidic cannabinoids was long overlooked. Issues of stability and a pharmacological focus on Δ^9-THC and its biological profile combined to relegate the non-narcotic native form of phytocannabinoids to a sort of investigational limbo. Recent studies have disclosed an attractive bioactivity profile for specific acidic phytocannabinoids but concerns about their limited stability have remained substantially unaddressed. To solve this issue, we have developed the hydroxamate derivatives of Δ^8-tetrahydrocannabinolic acid-A (Δ^8-THCA-AH, **6**) and cannabidiolic acid (CBDAH, **5**) as novel acidic cannabinoid bioisosteres, and we report here their synthesis and bioactivity profile against specific cannabinoid targets, as well as promising *in vivo* activity in a murine model of polycystic ovary syndrome (PCOS) associated with obesity.

KEYWORDS

acidic cannabinoids, hydroxamates, cannabinoid receptors, PPAR γ, obesity

1 Introduction

An acidic form of phytocannabinoids is produced in cannabis (*Cannabis sativa* L.) in accordance with their derivation from the aldol-type aromatization of an acidic polycarbonyl linear precursor (Hanuš et al., 2016). This seminal discovery was reported more than 50 years after the purification of cannabinol, the first phytocannabinoid to be obtained in pure form, thus testifying to the combination of technical and legal difficulties that have plagued phytocannabinoid research (Appendino, 2020). The presence of the *ortho*- and *para*-electron-releasing oxygen functions makes the native form of acidic phytocannabinoids prone to decarboxylation (Pollastro et al., 2017), a process slow at room temperature but dramatically accelerated by heating (Filer, 2022). In the early stages of bioactivity studies on phytocannabinoids, attention was largely focused on Δ^9-tetrahydrocannabinol (Δ^9-THC, **1a**) and compounds that shared its biological profile; the other phytocannabinoids were ignored. Since acidic cannabinoids are non-psychotropic and inactive in the tetrad test (Hanuš et al., 2016), their study was long neglected and only started in the wake of the demonstration of the clinical potential of cannabidiol (CBD, **2a**), the archetypal non-narcotic phytocannabinoid (Hanuš et al., 2016). Remarkable differences were evidenced between the biological profile of the neutral and the acidic forms of Δ^9-THC (Δ^9-THCA-A, **1b**) and of CBD (CBDA, **2b**), with significant changes in terms of orthosteric and allosteric interaction with CB_1R and increased emphasis on the

modulation of peroxisome proliferator-activated receptor-γ (PPARγ), GPR55 receptor, and ion channel-like transient receptor potential cation channel subfamily V member 1 (TRPV-1) [5]. Conversely, the interaction with CB_2R was largely retained (Caprioglio et al., 2022).

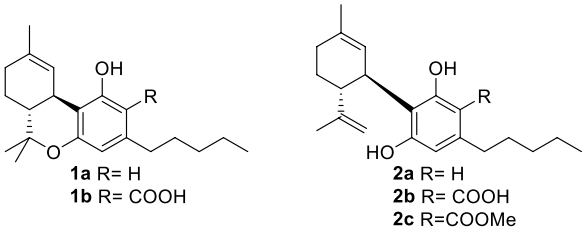

The decarboxylation of acidic phytocannabinoids is a non-enzymatic process triggered by physical agents (heat and light) and thermodynamically driven by the volatility of CO_2 (Filer, 2021). Under physiological conditions, the decarboxylation of acidic phytocannabinoids is slow when considered on a pharmacodynamic and pharmacokinetic time scale, with negligible generation of their neutral version (Filler, 2021; Filler, 2022). Therefore, the biological profile of acidic phytocannabinoids does not significantly overlap *in vivo* with their corresponding neutral derivatives. However, their intrinsic instability for decarboxylation means that special storage conditions are required, substantially hindering their pharmacological development both as pure compounds and extract constituents (Filer, 2021; Filer, 2022). The pharmacological potential of acidic phytocannabinoids has been validated in neuroprotection (Nadal et al., 2017), type-2 diabetes and metabolic syndrome-related conditions (Palomares et al., 2020b), non-alcoholic liver disease (Carmona-Hidalgo et al., 2021), and arthritis (Palomares et al., 2020a). Interestingly, the non-narcotic phytocannabinoid Δ^9-THCA-A modulates CB_1R receptor activity, acting as a positive allosteric modulator (PAM) (Palomares et al., 2020a).

The attractive biological profile of acidic phytocannabinoids has fostered research on solving the stability issue while preserving the key elements of their pharmacophore—an intramolecularly hydrogen-bonded carboxylic group C-2. Several strategies to stabilize acidic phytocannabinoids are, in principle, possible. Esterification of CBDA (**2b**) with methanol affords an ester (**2c**) is pharmacologically interesting but has an unclear relationship with the biological profile of the native natural product (Pertwee et al., 2018). Since the presence of a free carboxylic group is critical for high-affinity interaction with PPARγ and the allosteric binding site of CB_1R—both major targets of acidic phytocannabinoids (Nadal et al., 2017; Palomares et al., 2020b)—we explored stabilization alternatives capable of retaining an acidic functionality on the resorcinolic core.

2 Results and discussion

Hydroxamic acids (*N*-hydroxyamides) have long been known for their remarkable acidity compared to hydroxylamines (pKa ca 8–9 vs ca 14), a property that has generated a long debate on the location of the negative charge in their anions; it prevails on nitrogen in the gas phase and in non-polar solvents but on oxygen in polar solvents, at least when their acyl residue does not contain strongly electron-attracting substituents (Böhm and Exner, 2003). Unlike amides, hydroxamic acids therefore retain substantially more acidity than their corresponding acids, with a decrease of pKa limited 4–5 units (Citarella et al., 2021). Because of their outstanding chelating properties toward iron (III) and zinc (II), hydroxamic acids have been extensively used as metalloprotease inhibitors in drug discovery projects, with three hydroxamate-based histone deacetylase (HDAC) inhibitors currently approved as anti-cancer drugs (vorinostat, belinostat and anobinostat) for the treatment of lymphoma and multiple myeloma. In addition, another hydroxamate derivative (deferoxamine) is in clinical use for the management of iron overdose (Citarella et al., 2021). Since the hydroxamic function is stable toward decarboxylation, we have investigated the replacement of the carboxylic group of acidic phytocannabinoids with an hydroxamate group. The toxicological profile of hydroxamic acids, and particularly mutagenicity, is strongly dependent on their acyl moiety (Citarella et al., 2021), so we were therefore confident that the safety profile of phytocannabinoids (Dziwenka et al., 2020) could be preserved in the hydroxamate derivatives.

The hydroxamate derivative of CBDA (**2b**) was prepared in a three-step protocol (Scheme 1) involving protection of the two phenolic hydroxyls as the diacetates **3**, activation of the carboxylic group with the couple hydroxybenzotriazole (HOBt)-dicyclohexylcarbodiimide (DCC) (van Houten et al., 2012) to afford the benzotriazolyl hydroxamate **4**, and eventual reaction with hydroxylamine hydrochloride and triethylamine. This displaced hydroxybenzotriazole from the acyl group and the acetate-protecting groups from the phenolic hydroxyls of **4**, directly affording the globally deprotected hydroxamate **5** (overall yield from CBDA: 38%). Acidic treatment of **5** cyclized the *p*-methyl moiety into the hydroxamate analog of Δ^8-THCA-A (**6**), affording a second interesting candidate for biological evaluation (overall yield from CBDA: 10%). The ^{1}H- and ^{13}C NMR spectra of the hydroxamates were similar to that of their corresponding acids, the major difference being the expected upfield shift of the carbonyl group from *ca* 171–172 to 168–169.

Compared with their corresponding carboxylic acids (Nadal et al., 2017), both **5** and **6** showed a marked reduction of PPARγ activity but substantial PAM activity on CB_1R (Table 1). Additionally, **5** was inactive on GPR55 function, while **6** showed agonistic activity on this receptor, and both compounds behaved as TRPV-1 antagonists, albeit only at a relative high concentration (Table 1).

The *in vivo* activity of the hydroxamates **5** and **6** was tested in a well-validated mouse model of polycystic ovary syndrome (PCOS) (van Houten et al., 2012). PCOS is a highly prevalent condition which affects 6%–18% of women of reproductive age (Kataoka et al., 2017). Our preclinical model was generated by chronic exposure of female mice to dihydrotestosterone (DHT) from weaning onwards (i.e., post-weaning androgenization—PWA); this model phenocopies a subtype of women with this condition who suffer metabolic comorbidities (van Houten et al., 2012). PWA mice present important metabolic dysregulation, including traits of metabolic syndrome, and mimic some ovarian/hormonal characteristics of PCOS women (van Houten et al., 2012). To exacerbate the metabolic complications in this model, PWA mice were fed a high-fat content diet (HFD) for 18 weeks before initiation of the pharmacological treatments. This was considered appropriate for testing the metabolic effects of the cannabinoid hydroxamates,

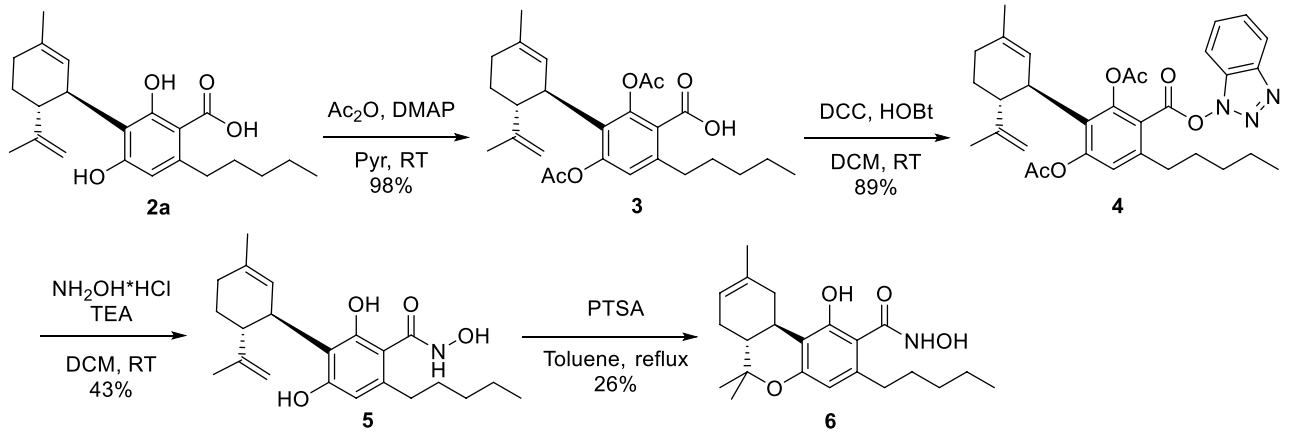

SCHEME 1
Synthesis of the hydroxamates **5** and **6**.

TABLE 1 ***In vitro*** **biological activities of cannabinoid hydroxamates.**

Compound	PPARγ activity	CB1 orthosteric agonism	CB1 antagonism	CB1 PAM	CB2 agonism	GPR55 agonism	TRPV-1 antagonism
5	>20 μM	Negative	Negative	1.48 ± 0.19 μM	Negative	Negative	16.61 ± 5.11 μM
6	>20 μM	Negative	Negative	2.47 ± 0.23 μM	Negative	11.84 ± 7.99 μM	18.13 ± 7.62 μM

PPARγ, peroxisome proliferator-activated receptor gamma; CB1, cannabinoid receptor type 1; CB2, cannabinoid receptor type 2; GPR55, G protein-coupled receptor 55; TRPV-1, transient receptor potential cation channel subfamily V member 1; PAM, positive allosteric modulator.

especially since PCOS is a prevalent condition for which developing effective therapies that target its metabolic comorbidities remains as an unmet medical need.

Postweaning androgenization worsened the metabolic profile caused by HFD alone as PWA mice displayed a ~30% increase of body weight (BW) vs. non-androgenized female mice fed with HFD before initiation of the treatments. Daily treatment with **5** or **6** for 28 days caused a clear reduction of BW through the treatment period, with a ~10%–15% drop in final BW after the 4-week administration (Figure 1A). In terms of body composition, PWA mice fed with HFD displayed a corresponding increase in total fat mass and adiposity index (defined as the quotient between fat mass and the sum of fat and lean mass), while a 4-week treatment with either **5** or **6** caused a clear reduction of both parameters, which was modestly higher in the case of **6** (Figures 1B, C). Remarkably, a substantial fraction of women with PCOS—which ranges between 38% and 88%, depending on the studies—are also obese (Barber and Franks, 2021), a condition recognized as one of the most common complications of the syndrome. Since a lowering of body weight remains one of the most effective first-line measures of tackling PCOS (Kataoka et al., 2017), our data provide a solid basis for the potential pharmacological use of cannabinoid hydroxamates in the integral management of women suffering from metabolic disorder in PCOS.

In addition, PWA mice fed a HFD also showed alterations in glycemic homeostasis reminiscent of those in the majority of women with PCOS (Barber and Franks, 2021). This is exemplified by increased basal glucose levels, worsened glucose tolerance, and reduced insulin sensitivity. Thus, the net increase in circulating glucose levels following i.p. injection of a glucose bolus was significantly higher in PWA mice than in non-androgenized controls, as revealed by GTT. Conversely, insulin sensitivity was decreased in our PCOS model, as denoted by smaller glucose-lowering responses to a bolus of exogenous insulin in ITT. In addition, these analyses demonstrated that treatment of PWA mice with the hydroxamates **5** or **6** significantly improved glucose tolerance, as shown by individual GTT profiles and by integral glucose changes estimated by AUC (area under curve) during the 120-min period following glucose injection (Figures 2A, B). Likewise, chronic treatment with **5** or **6** also improved insulin sensitivity as individual ITT time-course profiles were lower than those of PWA mice treated with vehicle (Figure 2C).

Together, our observations show that the beneficial effects of cannabinoid hydroxamates on the metabolic profile of the PCOS model are not restricted to their capacity to lower BW but also involve an improved glucose homeostasis. Given the potential side-effects of metformin as a first-line drug for managing insulin resistance in PCOS women, our data pave the way for future comparative analyses of the efficacy and safety of acidic cannabinoids in the treatment of insulin resistance—a common trait of women suffering this condition.

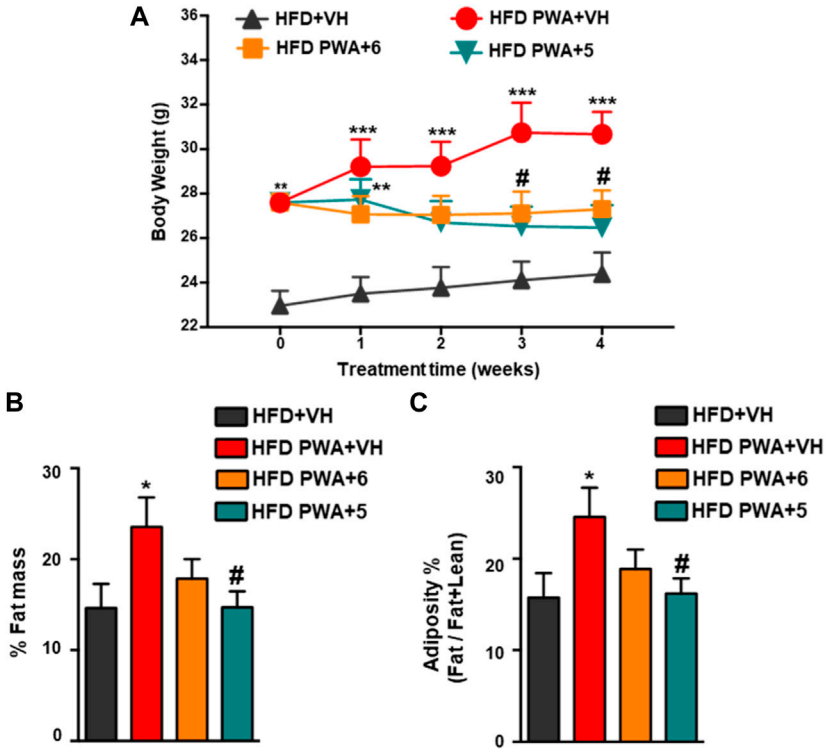

FIGURE 1
(A) Evolution of body weight (BW) during the 4-week treatment period in control mice fed with high-fat diet (HFD) and mice subjected to chronic exposure to dihydrotestosterone (DHT) from weaning onwards (PWA) and fed with HFD, treated for 28 days with vehicle (VEH), compound **5,** or compound **6**. For each experimental group, the sample size was seven animals per group. **(B)** Percentage of fat mass and **(C)** adiposity index, calculated as the ratio between fat mass and fat + lean mass at the end of treatments in the four experimental groups. $^{*}p < 0.05$, $^{**}p < 0.01$, $^{***}p < 0.001$ vs. HFD + VH mice; $^{\#}p < 0.05$, $^{\#\#}p < 0.01$, $^{\#\#\#}p < 0.001$ vs. HFD PWA + VH mice. Data are expressed as the mean +SEM. Two-way ANOVA followed by Tukey's test was used to determine statistical significance.

Δ^9-THCA-A, a functional CB_1R PAM (Palomares et al., 2020a), can ameliorate HFD-induced obesity and metabolic syndrome (Palomares et al., 2020b). The observation of a similar effect in cannabinoid hydroxamates shows that they can mimic a significant fraction of the biological profile of acidic cannabinoids, providing the first evidence that the instability issue of these compounds can be solved without detriment to their biological profile.

3 Experimental section

3.1 Chemistry

3.1.1 General

IR spectra were recorded on an Avatar 370 FT-IR Techno-Nicolet apparatus. ^{1}H (400 MHz) and ^{13}C (100 MHz) NMR spectra were measured on a Bruker Avance 400 MHz spectrometer. Chemical shifts were referenced to the residual solvent signal ($CDCl_3$: δH = 7.21, δC = 77.0). Homonuclear ^{1}H connectivities were determined by correlation spectroscopy (COSY). One-bond heteronuclear ^{1}H–^{13}C connectivities were determined by heteronuclear single quantum coherence (HSQC) spectroscopy. Two- and three-bond ^{1}H–^{13}C connectivities were determined by gradient two-dimensional (2D) heteronuclear multiple bond correlation (HMBC) optimized for $a^{2,3}J$ = 9 Hz. Low- and high-resolution electrospray ionization mass spectrometry (ESI-MS) data were determined on an LTQ OrbitrapXL (Thermo Scientific) mass spectrometer. Reactions were monitored by thin-layer chromatography (TLC) on Merck 60 F254 (0.25 mm) plates, visualized by staining with 5% H_2SO_4 in EtOH and heating. Organic phases were dried with Na_2SO_4 before evaporation. Chemical reagents and solvents were purchased from Sigma-Aldrich, TCI Europe, or Fluorochem and were used without further purification unless stated. Petroleum ether with a boiling point of 40°C–60°C was used. Silica gel 60 (70–230 mesh) was used for gravity column chromatography (GCC). All work-up solutions were dried with Na_2SO_4 before evaporation.

3.1.2 *N*-Hydroxycannabidiolcarboxamide (**5**)

3.1.2.1 Diacetylcannabidiolic acid (**3**)

An excess of acetic anhydride (105.8 mmol) and catalytic DMAP were added to a stirred solution of cannabidiolic acid [CDBA (**2b**), 1.88 g, 5.24 mmol)] in pyridine (10 mL). The reaction was stirred at room temperature overnight and then cooled to 0 °C (ice bath) and worked up by quenching with methanol (10 mL) to destroy the excess of acetic anhydride and dilution with EtOAc. The phases were separated, and the lower water phase was washed with EtOAc. The combined organic phases were then washed with 2*N* H_2SO_4 and

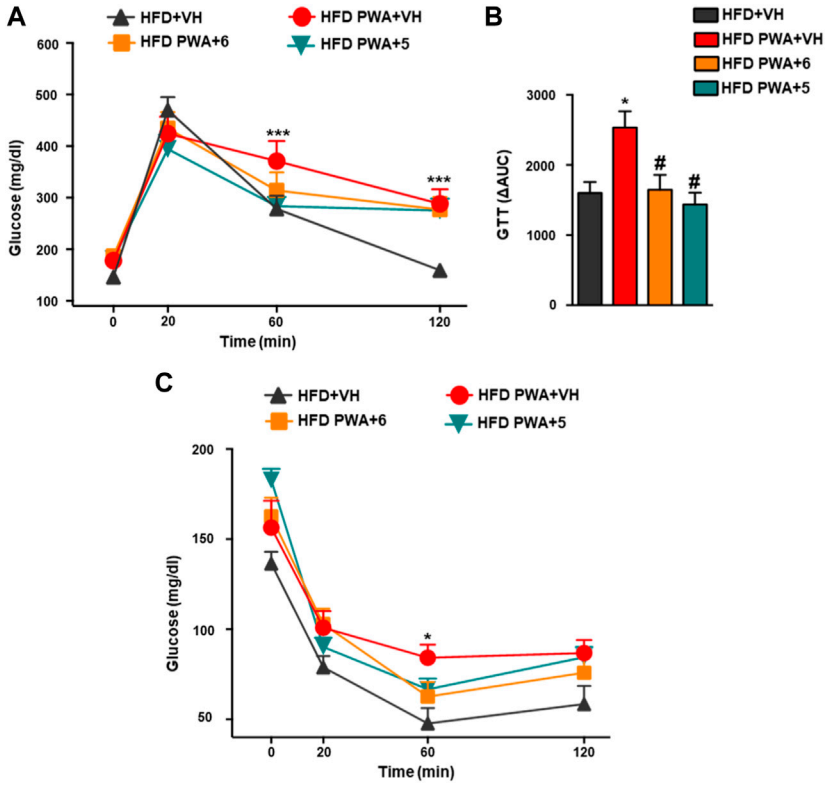

FIGURE 2
Glucose GTT; **(A)** insulin ITT; **(C)** tolerance tests applied to HFD or HFD + PWA mice treated for 4 weeks with compound **5**, compound **6**, or vehicle. In addition to individual time-point data, in the case of GTT, integral glucose responses, estimated as AUC by the trapezoidal rule, are shown **(B)**. Data presented as means +SEM of seven mice per group. $^{*}p < 0.05$, $^{**}p < 0.01$, $^{***}p < 0.001$ vs. HFD + VH group; $^{\#}p < 0.05$, $^{\#\#}p < 0.01$, $^{\#\#\#}p < 0.001$ vs. HFD PWA + VH group. Two-way ANOVA followed by Tukey's test was used to determine statistical significance.

eventually with brine. After drying and evaporation, the residue was purified by GCC on silica gel to afford 2.27 g (98%) **3** as white powder. IR (ν_{max} cm^{-1}): 2,958, 1764, 17,001 1,387, 1,162, 1,032, 885; ^{1}H NMR (400 MHz, $CDCl_3$): δ 6.87 (s, 1H), 5.23 (d, J = 2.8 Hz, 1H), 4.58 (t, J = 1.8 Hz, 1H), 4.48 (d, J = 2.2 Hz, 1H), 3.09–2.66 (m, 3H), 2.42–2.12 (m, 8H), 2.08 (dd, J = 4.5, 2.2 Hz, 1H), 1.85–1.70 (m, 2H), 1.70 (s, 3H), 1.68–1.59 (m, 2H), 1.61 (s, 3H), 1.42–1.23 (m, 4H), and 1.01–0.79 (m, 3H); ^{13}C NMR (100 MHz, $CDCl_3$) δ 171.90, 169.02, 168.62, 151.38, 148.52, 147.31, 141.99, 133.34, 127.80, 123.91, 122.88, 111.50, 45.48, 38.71, 33.68, 31.67, 30.68, 30.39, 28.58, 23.43, 22.37, 20.92, 20.71, 19.37, and 13.97. HRESIMS *m/z* [M + Na]$^{+}$ 465.2241 (calcd for $C_{26}H_{34}NaO_6$, 465.2253).

3.1.2.2 Diacetylhydroxybenzotriazolycannabidiolic acid (**4**)

Dicyclohexylcarbodiimide (DCC, 1.21 g, 5.88 mmol, 2 mol. equiv.) and hydroxybenzotriazole (HOBt) (0.79 g, 5.88 mmol, 2 mol. equiv.) were sequentially added to a stirred solution of diacetyl-CBDA (**3**, 1.30 g, 2.94 mmol) in dry DCM (10 mL). The mixture was stirred at room temperature for 90 min until TLC showed complete consumption of the starting material (product *Rf* = 0.82, PE/EtOAC 9:1). The solvent was then evaporated, and the residue was dissolved in toluene and cooled at −18°C overnight to remove dicyclohexylurea (DCU) as a white precipitate. After filtration, the organic phase was washed with brine, then dried and evaporated. The residue was purified by GCC on silica gel to afford 1.46 g (89%) of benzotriazole derivative **4** as a yellowish oil. IR (ν_{max} cm^{-1}): 2,927, 1771, 1700, 1,366, 1,171, 1,075, and 740; ^{1}H NMR (400 MHz, $CDCl_3$): δ 8.10 (d, J = 8.5 Hz, 1H), 7.62–7.54 (m, 2H), 7.45 (t, J = 8.2 Hz, 1H), 6.99 (s, 1H), 5.24 (s, 1H), 4.60 (d, J = 1.8 Hz, 1H), 4.50 (s, 1H), 3.05–2.81 (m, 2H), 2.80–2.66 (m, 1H), 2.45–2.14 (m, 7H), 2.10–2.02 (m, 1H), 1.89–1.72 (m, 2H), 1.71 (s, 3H), 1.63 (s, 3H), and 0.89 (t, J = 7.0 Hz, 3H); ^{13}C NMR (100 MHz, $CDCl_3$): δ 171.16, 168.38, 162.80, 152.86, 149.23, 147.13, 143.53, 142.98, 133.88, 128.86, 128.81, 124.86, 123.46, 120.56, 111.75, 108.44, 60.40, 53.44, 45.52, 38.81, 34.00, 31.65, 31.01, 30.38, 28.50, 23.48, 22.43, 21.06, 20.93, 20.86, 19.39, 17.72, 14.21, 13.99, and 12.30. HRESIMS *m/z* [M + Na]$^{+}$ 582.2571 (calcd for $C_{32}H_{37}N_3NaO_6$, 582.2580).

3.1.2.3 N-Hydroxycannabidiolcarboxamide (**5**)

Hydroxylamine hydrochloride (0.73 g, 10.43 mmol, 4 mol. equiv.) and triethylamine (TEA, 1.45 mL, 10.43 mmol, 4 mol. equiv.) were added to a stirred solution of **4** (1.46 g, 2.60 mMol) in DCM (50 mL). The solution was stirred at room temperature for 24 h and then quenched with 2*N* H_2SO_4 and diluted with DCM. The combined organic phases were washed with brine, then dried and evaporated, and the residue was purified by GCC on silica gel to afford 0.42 g (43%) **5** as a dark-colored oil. IR (ν_{max} cm^{-1}): 3,247, 3,071, 2,926, 1738, 1,603, 1,370, 1,196, 1,040, and 838; ^{1}H NMR (400 MHz, $CDCl_3$): δ 6.26 (s, 1H), 5.52 (s, 1H), 4.54 (s, 1H), 4.40 (s, 1H), 4.04 (m, 1H), 2.65

(t, J = 7.8 Hz, 2H), 2.47–2.35 (m, 1H), 2.33–2.16 (m, 1H), 2.16–2.04 (m, 1H), 1.87–1.75 (m, 5H), 1.69 (s, 3H), 1.58 (m, 2H), 1.38–1.24 (m, 4H), and 0.87 (t, J = 7.8 Hz, 3H); ^{13}C NMR (100 MHz, $CDCl_3$) δ 169.15, 159.20, 159.00, 147.37, 140.49, 123.74, 115.26, 111.30, 110.63, 105.95, 46.56, 35.59, 34.59, 31.64, 30.81, 30.26, 27.88, 23.73, 22.44, 18.93, 17.69, and 13.98. HRESIMS m/z $[M + Na]^+$ 396.2179 (calcd for $C_{22}H_{31}NNaO_4$, 396.2151).

3.1.3 Δ8-N-Hydroxytetrahydrocannabinolcarboxamide (6)

PTSA (17 mg, 0.100 mmol, 0.2 mol equiv) was added to a stirred solution of **5** (120 mg, 0.50 mmol) in toluene (2 mL). The mixture was heated to 120°C for 2 h, cooled, and then quenched by the addition of sat. $NaHCO_3$ and diluted with EtOAc. The organic phase was washed with brine, then dried and evaporated, and the residue was purified by GCC on silica gel to afford 32 mg (26%) **6** as a dark-colored oil. IR (ν_{max} cm^{-1}): 3,253, 3,058, 2,938, 1740, 1,582, 1,315, and 1,212, 846; ^{1}H NMR (400 MHz, $CDCl_3$): δ 6.52 (s, 1H), 5.56–5.39 (m, 1H), 3.13 (dd, J = 17.1, 5.1 Hz, 1H), 2.85 (td, J = 11.1, 5.0 Hz, 1H), 2.62 (t, J = 7.6 Hz, 3H), 2.22–2.12 (m, 1H), 2.07–1.78 (m, 4H), 1.76 (s, 3H), 1.73–1.61 (m, 3H), 1.41 (s, 6H), 1.36 (m, 4H), 1.12 (s, 3H), and 1.00–0.84 (t, J = 6.9 Hz, 3H); ^{13}C NMR (100 MHz, $CDCl_3$) δ 157.26, 149.53, 142.04, 133.96, 124.27, 121.20, 119.52, 112.75, 108.33, 77.26, 43.26, 35.33, 31.36, 30.77, 30.54, 29.21, 27.55, 27.32, 23.43, 22.54, 18.68, and 13.99. HRESIMS m/z $[M + Na]^+$ 396.2180 (calcd for $C_{22}H_{31}NNaO_4$, 396.2151).

3.2 Biological evaluation

3.2.1 Determination of PPARγ activity

HEK-293T cells were seeded in 24-well plates (10^5 cells/well) and transiently co-transfected with the expression vector GAL4-PPARγ (20 ng/mL), the luciferase reporter vector GAL4-Luc (20 ng/mL), and the pRL-CMV vector (50 ng/mL) using Roti©-Fect (Carl Roth, Karlsruhe, Germany) following the manufacturer's instructions. The transfected cells were treated 24 hours later with increasing concentrations of the compounds for 6 h. The cells were then lysed, and luciferase activity was measured using the Dual-Luciferase® reporter assay system (Promega; Madison, WI, United States). The compounds were tested at 1, 5, 10, 20, and 40 μM (Supplementary Material).

3.2.2 CB1 receptor (CB1R) and CB2 receptor (CB2R) functional assays

For CB_1R agonism, antagonism, and PAM activities, HEK293T-CB1 cells transiently transfected with the plasmid CRE-Luc (0.2 μg) harboring six consensus cAMP responsive elements linked to firefly luciferase reporter gene were used as previously described (Salamone et al., 2021). For CB_2R agonism, HEK293T-CB2 cells transiently transfected with the plasmid CRE-Luc (0.2 μg) were used as previously described (del Río et al., 2016). The compounds were tested at 1, 5, 10, 20, and 40 μM (Supplementary Material).

3.2.3 GPR55 functional assays

The determination of GPR55 agonistic activity was carried out using HEK293T-GPR55 cells transiently transfected with the plasmid CRE-Luc (0.2 μg), as previously described (Apweiler et al., 2022). The compounds were tested at 1, 5, 10, 20, and 40 μM (Supplementary Material).

3.2.4 TRPV-1 functional assays

HEK293T-TRPV-1 cells (2×10^4/well) were cultured in triplicate in 96-well microtiter plates in 200 μL of complete medium. The cells were incubated with the compounds for 30 min and then stimulated with the agonist capsaicin (3 μM) for 6 h. Capsazepine was used as the positive control for TRPV-1 antagonism. Capsaicin-induced cytotoxicity was measured by the standard MTT method. The results represent the activity of **6a** and **7** to prevent capsaicin-induced cytotoxicity. The compounds were tested at 1, 5, 10, 20, and 40 μM (Supplementary Material).

3.2.5 Murine model of PCOS

A well-validated mouse model (C57BL6J strain) of post-weaning androgenization (named hereafter PWA) was used (Caldwell et al., 2014). To achieve chronic exposure to high levels of androgens, female mice were implanted at the time of weaning (postnatal day 21; PND21) with subcutaneous capsules, composed of SILASTIC brand silicon tubing elastomers (Dow Corning, Midland, MI; 10 mm length; inner diameter, 0.062 cm; exterior diameter, 0.125 cm) containing about 10 mg of DHT. We had previously conducted validation analyses that confirmed that silastic capsules would ensure constant release and elevated levels of DHT over our period of experimentation (Romero-Ruiz et al., 2019). Control mice were fed empty capsules. All animals were maintained under a 12-h light/dark cycle at standard temperature (21oC ± 2°C) and given *ad libitum* access to diet (see below) and water. To ensure constant exposure to high levels of DHT, capsules were replaced at PND90, thereby allowing maintenance of a constant release of the androgen. Given the focus of our studies, this model in our experiments was given a HFD, D12451 (45%, 20%, and 35% calories from fat, protein, and carbohydrate, respectively from Research Diets Inc., New Brunswick, NJ, United States) in order to exacerbate the metabolic and hepatic alterations of PWA mice. For reference purposes, control (non-androgenized) mice, implanted with empty capsules, were also fed a HFD. All experimental procedures in this study were approved by the Ethical Committee of the University of Córdoba and the Junta de Andalucía (Spain); ref# 18/09/2017/132; all experiments were conducted in accordance with European Union (EU) norms for the use and care of experimental animals (EU Directive 2010/63/UE, September 2010).

3.2.6 Testing the effects of acidic cannabinoid compounds in PWA mice

The effects of chronic treatment with the acidic cannabinoid compounds **5** and **6** were assessed after chronic administration to PWA mice fed a HFD. Pharmacological treatments were started at a period of intervention when the animals already displayed overt metabolic and liver alterations. For *in vivo* testing, the experimental groups were defined (N ≥ 7) as follows: (1) control group fed on HFD + vehicle; (2) PWA mice fed on HFD + vehicle; (3) PWA mice fed on HFD + compound **5** (20 mg/Kg); (4) PWA mice fed on HFD + compound **6** (20 mg/Kg). Mice were administered either with vehicle or the corresponding dose of the compounds for 28 days by daily intraperitoneal injection (i.p) starting at week 18 after initiation of

45% HFD. Treatments were initiated after 18 weeks of feeding with HFD. Metabolic parameters were monitored throughout the treatment, including body weight and composition, glucose tolerance (GTT), and insulin sensitivity (ITT).

3.2.7 Intraperitoneal glucose and insulin tolerance tests, and body composition analyses

For glucose tolerance tests (GTT), animals were i.p. injected with a bolus of 2 g of glucose per kg body weight (BW) after a 5-h period of food deprivation; blood glucose levels were determined at 0 (basal), 20, 60, and 120 min after injection. For insulin tolerance tests (ITT), the animals were subjected to i.p. injection of 0.75 international units (IU) of insulin (Sigma-Aldrich) per kg BW after a 5-h fasting. Blood glucose levels were measured at 0 (basal), 20, 60, and 120 min. All glucose concentrations were measured using a handheld glucometer (Accu-Chek Advantage®; Roche Diagnostics). Body composition analyses were performed by quantitative magnetic resonance (QMR) using the EchoMRI™ 700 analyzer (Houston, TX, software v.2.0).

3.2.8 Statistical analyses

Data were analyzed using Prism software (GraphPad Prism version 8.00 for Macintosh, GraphPad Software, La Jolla, California, United States, https://www.graphpad.com/). For animal experiments, mice were assigned to different treatment groups by stratified randomization within each model (HFD vs. HFD + PWA), ensuring similar mean body weights within comparative groups. However, for operational reasons, the groups were not blinded to the experimenters. In any event, whenever possible, primary data analyses by senior authors were carried out independently to minimize any bias. *In vivo* data are expressed as the mean ± SEM. Two-way ANOVA followed by Tukey's *post hoc* test was used to determine statistical significance; the level of significance was set at $p < 0.05$.

Data availability statement

The original contributions presented in the study are included in the article/Supplementary Material; further inquiries can be directed to the corresponding authors.

Ethics statement

The animal study was reviewed and approved by the Ethical Committee of the University of Córdoba and Junta de Andalucía (Spain); ref# 18/09/2017/132 European Union (EU) normative for the use and care of experimental animals (EU Directive 2010/63/UE, September 2010).

Author contributions

GA, EM, and DC conceived and designed the experiments. HIMA, DC, FR-P, and JC performed the experiments. HIMA, FR-P, JC, GA, MT-S, and EM analyzed the data. DC, GA, and EM contributed to the writing of the manuscript. All authors contributed to the article and approved the submitted version.

Funding

Work in Novara was also supported by MIUR (PRIN 2017, Project 2017WN73PL, Bioactivity-directed exploration of the phytocannabinoid chemical space). The authors gratefully acknowledge the financial support from Skye Bioscience (San Diego, United States).

Conflict of interest

The author DC declared that they were an editorial board member of Frontiers at the time of submission. This had no impact on the peer review process and the final decision.

The remaining authors declare that the research was conducted in the absence of any commercial or financial relationships that could be construed as a potential conflict of interest.

Publisher's note

Supplementary material

The Supplementary Material for this article can be found online at: https://www.frontiersin.org/articles/10.3389/fntpr.2023.1190053/full#supplementary-material

References

Appendino, G. (2020). The early history of cannabinoid research. *Rend. Fis. Acc. Lincei* 31, 919–929. doi:10.1007/s12210-020-00956-0

Apweiler, M., Streyczek, J., Saliba, S. W., Collado, J. A., Hurrle, T., Gräßle, S., et al. (2022). Functional selectivity of coumarin derivates acting via GPR55 in neuroinflammation. *IJMS* 23, 959. doi:10.3390/ijms23020959

Barber, T. M., and Franks, S. (2021). Obesity and polycystic ovary syndrome. *Clin. Endocrinol.* 95, 531–541. doi:10.1111/cen.14421

Böhm, S., and Exner, O. (2003). Acidity of hydroxamic acids and amides. *Org. Biomol. Chem.* 1, 1176–1180. doi:10.1039/b212298g

Caldwell, A. S. L., Middleton, L. J., Jimenez, M., Desai, R., McMahon, A. C., Allan, C. M., et al. (2014). Characterization of reproductive, metabolic, and endocrine features of polycystic ovary syndrome in female hyperandrogenic mouse models. *Endocrinology* 155, 3146–3159. doi:10.1210/en.2014-1196

Caprioglio, D., Amin, H. I. M., Taglialatela-Scafati, O., Muñoz, E., and Appendino, G. (2022). Minor phytocannabinoids: A misleading name but a promising opportunity for biomedical research. *Biomolecules* 12, 1084. doi:10.3390/biom12081084

Carmona-Hidalgo, B., González-Mariscal, I., García-Martín, A., Prados, M. E., Ruiz-Pino, F., Appendino, G., et al. (2021). Δ9-Tetrahydrocannabinolic Acid markedly

alleviates liver fibrosis and inflammation in mice. *Phytomedicine* 81, 153426. doi:10.1016/j.phymed.2020.153426

Citarella, A., Moi, D., Pinzi, L., Bonanni, D., and Rastelli, G. (2021). Hydroxamic acid derivatives: From synthetic strategies to medicinal chemistry applications. *ACS Omega* 6, 21843–21849. doi:10.1021/acsomega.1c03628

del Río, C., Navarrete, C., Collado, J. A., Bellido, M. L., Gómez-Cañas, M., Pazos, M. R., et al. (2016). The cannabinoid quinol VCE-004.8 alleviates bleomycin-induced scleroderma and exerts potent antifibrotic effects through peroxisome proliferator-activated receptor-γ and CB2 pathways. *Sci. Rep.* 6, 21703. doi:10.1038/srep21703

Dziwenka, M., Coppock, R., Alexander, M., Palumbo, E., Ramirez, C., and Lermer, S. (2020). Safety assessment of a hemp extract using genotoxicity and oral repeat-dose toxicity studies in sprague-dawley rats. *Toxicol. Rep.* 7, 376–385. doi:10.1016/j.toxrep.2020.02.014

Filer, C. N. (2022). Acidic cannabinoid decarboxylation. *Cannabis Cannabinoid Res.* 7, 262–273. doi:10.1089/can.2021.0072

Filer, C. N. (2021). On the reluctant decarboxylation of thca-b. *Cannabis And Cannabinoid Research* 6, 446–448. doi:10.1089/can.2021.0003

Hanuš, L. O., Meyer, S. M., Muñoz, E., Taglialatela-Scafati, O., and Appendino, G. (2016). Phytocannabinoids: A unified critical inventory. *Nat. Prod. Rep.* 33, 1357–1392. doi:10.1039/C6NP00074F

Kataoka, J., Tassone, E., Misso, M., Joham, A., Stener-Victorin, E., Teede, H., et al. (2017). Weight management interventions in women with and without PCOS: A systematic review. *Nutrients* 9, 996. doi:10.3390/nu9090996

Nadal, X., del Río, C., Casano, S., Palomares, B., Ferreiro-Vera, C., Navarrete, C., et al. (2017). Tetrahydrocannabinolic acid is a potent PPARγ agonist with neuroprotective activity: Cannabinoid acids are PPARγ agonists. *Br. J. Pharmacol.* 174, 4263–4276. doi:10.1111/bph.14019

Palomares, B., Garrido-Rodriguez, M., Gonzalo-Consuegra, C., Gómez-Cañas, M., Saen-oon, S., Soliva, R., et al. (2020a). Δ^{9}-Tetrahydrocannabinolic acid alleviates collagen-induced arthritis: Role of PPARγ and CB_1 receptors. *Br. J. Pharmacol.* 177, 4034–4054. doi:10.1111/bph.15155

Palomares, B., Ruiz-Pino, F., Garrido-Rodriguez, M., Eugenia Prados, M., Sánchez-Garrido, M. A., Velasco, I., et al. (2020b). Tetrahydrocannabinolic acid A (THCA-A) reduces adiposity and prevents metabolic disease caused by diet-induced obesity. *Biochem. Pharmacol.* 171, 113693. doi:10.1016/j.bcp.2019.113693

Pertwee, R. G., Rock, E. M., Guenther, K., Limebeer, C. L., Stevenson, L. A., Haj, C., et al. (2018). Cannabidiolic acid methyl ester, a stable synthetic analogue of cannabidiolic acid, can produce 5-HT_{1A} receptor-mediated suppression of nausea and anxiety in rats: HU-580, CBDA, 5-HT_{1A} receptor, nausea and anxiety. *Br. J. Pharmacol.* 175, 100–112. doi:10.1111/bph.14073

Pollastro, F., De Petrocellis, L., Schiano-Moriello, A., Chianese, G., Heyman, H., Appendino, G., et al. (2017). Amorfrutin-type phytocannabinoids from Helichrysum umbraculigerum. *Fitoterapia* 123, 13–17. doi:10.1016/j.fitote.2017.09.010

Romero-Ruiz, A., Skorupskaite, K., Gaytan, F., Torres, E., Perdices-Lopez, C., Mannaerts, B. M., et al. (2019). Kisspeptin treatment induces gonadotropic responses and rescues ovulation in a subset of preclinical models and women with polycystic ovary syndrome. *Hum. Reprod.* 34, 2495–2512. doi:10.1093/humrep/dez205

van Houten, E. L. A. F., Kramer, P., McLuskey, A., Karels, B., Themmen, A. P. N., and Visser, J. A. (2012). Reproductive and metabolic phenotype of a mouse model of PCOS. *Endocrinology* 153, 2861–2869. doi:10.1210/en.2011-1754